Quenching of para-H$_2$ with an ultracold antihydrogen atom $\overline{\text{H}}_{1s}$

Renat A. Sultanov,[1,*] Sadhan K. Adhikari,[2,†] and Dennis Guster[1,‡]

[1]*High Performance Computing Group, BCRL, St. Cloud State University, St. Cloud, Minnesota 56301-4498, USA*

[2]*Institute of Theoretical Physics, UNESP—Universidade Estadual Paulista, 01140-070 São Paulo, SP, Brazil*

In this work we report the results of calculation for quantum-mechanical rotational transitions in molecular hydrogen, H$_2$, induced by an ultracold ground-state antihydrogen atom $\overline{\text{H}}_{1s}$. The calculations are accomplished using a nonreactive close-coupling quantum-mechanical approach. The H$_2$ molecule is treated as a rigid rotor. The total elastic-scattering cross section $\sigma_{\text{el}}(\epsilon)$ at energy ϵ, state-resolved rotational transition cross sections $\sigma_{jj'}(\epsilon)$ between states j and j', and corresponding thermal rate coefficients $k_{jj'}(T)$ are computed in the temperature range 0.004 K $\lesssim T \lesssim$ 4 K. Satisfactory agreement with other calculations (variational) has been obtained for $\sigma_{\text{el}}(\epsilon)$.

I. INTRODUCTION

Interaction and collisional properties between matter and antimatter is of fundamental importance in physics [1,2]. The antihydrogen atom ($\overline{\text{H}}$), which is a bound state of an antiproton p^- and a positron e^+, is the simplest representative of an antimatter atom. This is a two-particle system, which, however, may possess very different interactional and dynamical properties compared to its matter counterpart: the H atom [3,4].

By now much effort has been exerted in various experiments to build and store $\overline{\text{H}}$ at cold and ultracold temperatures [5–9]. New experiments are planned or are in progress to test the fundamental laws and theories of physics involving antiparticles and antimatter in general [2]. For example, it follows from the charge conjugation, parity, and time reversal (CPT) symmetry of quantum electrodynamics that a charged particle and its antiparticle should have equal and opposite charges and equal masses, lifetimes, and gyromagnetic ratios. The CPT symmetry predicts that hydrogen and antihydrogen atoms should have identical spectra. Future experimentalists plan to test whether in fact H and $\overline{\text{H}}$ have such properties. Specifically, a starting point would be to compare the frequency of the 1s-2s two-photon transition in H and $\overline{\text{H}}$. Also, one of the important practical applications of antihydrogen has been mentioned in Ref. [10], where the authors considered controlled $\overline{\text{H}}$ propulsion for NASA's future plans in very deep space. Researchers at CERN [1] and from other groups [8] are interested to trap and study $\overline{\text{H}}$ at low temperatures, e.g., $T \lesssim 1$ K, when the $\overline{\text{H}}$ atom will be almost in its rest frame. The study of Lamb shift and response of antihydrogen to gravity at ultralow energies should allow them to test more precisely the predictions of two fundamental theories of modern physics: quantum field theory and Einstein's general theory of relativity [11].

It has been pointed out [12,13] that the main cause of loss of the $\overline{\text{H}}$ atoms confined in a magnetic gradient trap is due to $\overline{\text{H}} + \text{H}_2$ and $\overline{\text{H}} + \text{He}$ collisions. Therefore, the $\overline{\text{H}} + \text{H}_2$ scat-

tering cross sections and corresponding rotational-vibrational thermal rate coefficients, in the case of H$_2$, would be very helpful to gain a practical understanding of the slowing down and trapping of $\overline{\text{H}}$. Hence the investigation of the possibility of cooling of $\overline{\text{H}}$ atoms by colliding them with colder H$_2$ is of significant practical interest [14]. (Similar collision between trapped fermionic atoms with cold bosonic atoms has been fundamental in cooling the fermionic atoms and thus leading them to quantum degeneracy [15].) Such investigation of $\overline{\text{H}}$ interaction with H and H$_2$ can reveal the survival conditions of $\overline{\text{H}}$ in collisions with H and, even more importantly, with H$_2$ [16].

Further, cooling occurs by energy transfer in elastic collisions of $\overline{\text{H}}$ with H$_2$. However, during the collision, the rearrangement process may lead to the formation of protonium (pp^-) and positronium (e^+e^-) exotic atoms and the destruction of $\overline{\text{H}}$ atoms. They are formed as matter-antimatter bound states, which then annihilate. (There have also been many studies of scattering of positronium atoms [17], the lightest matter-antimatter atom). Thus one can conclude that the effectiveness of the cooling of $\overline{\text{H}}$ is determined from a comparison of the cross sections for direct scattering and rearrangement.

By now a series of theoretical works have been published, in which the properties of interaction between $\overline{\text{H}}$ and H, He, and H$_2$ have been investigated [12,18–20]. Some theoretical studies have been carried out for the $\overline{\text{H}} + \text{H}$ system at thermal energies using quantum-mechanical methods [21–26]. Also, discussions on the importance and applications for this system, especially in connection with Bose-Einstein condensation [27], ultracold collisions [16,22], and its static and dynamic properties [28], can be found in the literature.

In this work we present results for the collision of an ultracold $\overline{\text{H}}$ atom with H$_2$, where H$_2$ is treated as a rigid rotor with a fixed distance between hydrogen atoms. The elastic, rotational state-resolved scattering cross sections for the $\overline{\text{H}} - \text{H}_2$ scattering and their corresponding thermal rate coefficients are calculated using a nonreactive quantum-mechanical close-coupling approach. The potential interaction between $\overline{\text{H}}$ and the hydrogen atoms is taken from Ref. [18].

In Sec. II we present the basic quantum-mechanical scattering equations used in this work, present their partial-wave projection and scattering boundary conditions. The

---

*rasultanov@stcloudstate.edu; r.sultanov2@yahoo.com

†adhikari@ift.unesp.br; URL: http://www.ift.unesp.br/users/adhikari/

‡dcguster@stcloudstate.edu

expressions for transfer and elastic cross sections and transition rate coefficients are also given. The detail of the potential energy surface (PES) employed in the calculation is also provided. The numerical results and discussion are presented in Sec. III. We present a detailed account of the convergence of the numerical calculation with respect to different scattering and computational parameters. After assuring convergence in our calculations, we present the results of our numerical calculation involving elastic/inelastic scattering and transfer rates at ultralow energies on the $\overline{\text{H}}$ + para-H$_2$ system. Conclusions and a summary are provided in Sec. IV.

II. $\overline{\text{H}} - \text{H}_2$ SCATTERING FORMULATION

A. Basic equations

In this section we describe the close-coupling quantum-mechanical approach we used to calculate the cross sections and collision rates of a hydrogen molecule H$_2$ with an antihydrogen atom $\overline{\text{H}}$. Atomic units ($e = m_e = \hbar = 1$) are used in this section, where e and m_e are the charge and mass of an electron. Three-body Jacobi coordinates $\{\vec{r}, \vec{R}\}$ for the $\overline{\text{H}} + \text{H}_2(j)$ system used in this work are shown in Fig. 1. The two H atoms are labeled 2 and 3 and the $\overline{\text{H}}$ atom is labeled 1, O is the center of mass of the H$_2$ molecule, Θ is the polar angle between vector $\vec{r}$ connecting the two H atoms in H$_2$ (labeled 2 and 3) and vector $\vec{R}$ connecting the center of mass of the H$_2$ molecule to the $\overline{\text{H}}$ atom (labeled 1). Next, $\vec{j}$ and $\vec{L}$ are angular momenta corresponding to the vectors $\vec{r}$ and $\vec{R}$, respectively. The quantities x_{21} and x_{31} are the distances between the $\overline{\text{H}}$ atom labeled 1 and the H atoms labeled 2 and 3, respectively.

The Schrödinger equation for an $a + bc$ collision in the center-of-mass frame, where a ($\overline{\text{H}}$) is an atom and bc ($\overline{\text{H}}_2$) is a linear rigid rotor, is [29,30]

$$\left[\frac{P_{\vec{R}}^2}{2M_R} + \frac{L_{\hat{r}}^2}{2\mu r^2} + V(\vec{r}, \vec{R}) - E \right] \Psi(\hat{r}, \vec{R}) = 0, \quad (1)$$

where $P_{\vec{R}}$ is the relative momentum between a and bc; M_R is the reduced mass of the atom-molecule (rigid rotor in this model) system $a + bc$: $M_R = m_a(m_b + m_c)/(m_a + m_b + m_c)$; μ is the reduced mass of the target: $\mu = m_b m_c/(m_b + m_c)$; $\hat{r}$ is the angle of orientation of the rotor ab; $V(\vec{r}, \vec{R})$ is the PES for the three-atom system abc; and E is the total energy of the system. The eigenfunctions of the operator $L_{\hat{r}}^2$ in Eq. (1) are the spherical harmonics $Y_{jm}(\hat{r})$.
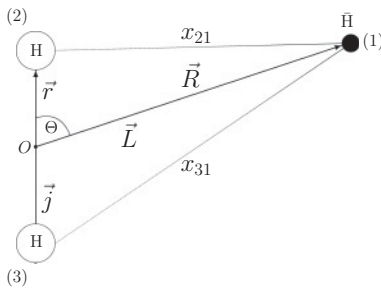

FIG. 1. Three-body Jacobi coordinates $\{\vec{r}, \vec{R}\}$ for the $\overline{\text{H}} + \text{H}_2(j)$ system used in this work.

To solve Eq. (1), the following expansion is used [31]:

$$\Psi(\hat{r}, \vec{R}) = \sum_{JMjL} \frac{U_{jL}^{JM}(R)}{R} \phi_{jL}^{JM}(\hat{r}, \vec{R}), \quad (2)$$

where channel expansion functions are

$$\phi_{jL}^{JM}(\hat{r}, \vec{R}) = \sum_{m_1 m_2} C_{jm_1 Lm_2}^{JM} Y_{jm_1}(\hat{r}) Y_{Lm_2}(\hat{R}), \quad (3)$$

where $\vec{J} = \vec{j} + \vec{L}$ is the total angular momentum of the system abc; M is its projection onto the space fixed z axis; m_1 and m_2 are projections of j and L, respectively; $C_{jm_1 Lm_2}^{JM}$ are the Clebsch-Gordan coefficients; and U's are the appropriate radial functions.

Substitution of Eq. (2) into Eq. (1) provides a set of coupled second-order differential equations for the unknown radial functions $U_{jL}^{JM}(R)$

$$\left(\frac{d^2}{dR^2} - \frac{L(L+1)}{R^2} + k_{jL}^2 \right) U_{jL}^{JM}(R)$$
$$= 2M_R \sum_{j'L'} \int \langle \phi_{jL}^{JM}(\hat{r}, \vec{R}) | V(\vec{r}, \vec{R}) | \phi_{j'L'}^{JM}(\hat{r}, \vec{R}) \rangle$$
$$\times U_{j'L'}^{JM}(R) d\hat{r} d\hat{R}. \quad (4)$$

To solve the coupled radial Eq. (4), we apply the hybrid modified log-derivative-Airy propagator in the general purpose scattering program MOLSCAT [32]. Additionally, we tested other propagator schemes included in MOLSCAT. Our calculations reveal that other propagators can also produce quite stable results.

The log-derivative matrix is propagated to large intermolecular distances R, since all experimentally observable quantum information about the collision is contained in the asymptotic behavior of functions $U_{jL}^{JM}(R \rightarrow \infty)$. The numerical results are matched to the known asymptotic behavior of $U_{jL}^{JM}(R)$ relating to the the physical scattering S matrix [33]

$$U_{jL}^{JM} \underset{R \rightarrow +\infty}{\sim} \delta_{jj'} \delta_{LL'} e^{-i[k_\alpha R - (L\pi/2)]}$$
$$- \left(\frac{k_\alpha}{k_{\alpha'}} \right)^{1/2} S^J(j'L'; jL; E) e^{i[k_{\alpha'} R - (L'\pi/2)]}, \quad (5)$$

where $k_\alpha = [2M_R(E - E_\alpha)]^{1/2}$ is the channel wave number of channel $\alpha = (jL)$, E_α is rotational channel energy, and E is the total energy in the abc system. This method was used for each partial wave until a converged cross section was obtained. It was verified that the results have converged with respect to the number of partial waves as well as the matching radius, $R_{\max}$, for all channels included in our calculations.

Cross sections for rotational excitation and relaxation phenomena can be obtained directly from the S matrix. In particular, the cross sections for excitation from $j \rightarrow j'$ summed over the final m' and averaged over the initial m are given by [31]

$$\sigma(j', j, \epsilon)$$
$$= \frac{\pi}{(2j+1)k_\alpha^2} \sum_{JLL'} (2J+1)|\delta_{jj'}\delta_{LL'} - S^J(j'L'; jL; E)|^2. \quad (6)$$

The kinetic energy is $\epsilon = E - B_e j(j+1)$, where B_e is the rotation constant of the rigid rotor bc, i.e., the hydrogen molecule.

The relationship between the rate coefficient $k_{j \to j'}(T)$ and the corresponding cross section $\sigma_{j \to j'}(E_{\rm kin})$ can be obtained through the following weighted average [34]

$$k_{j \to j'}(T) = \sqrt{\frac{8 k_B T}{\pi M_R}} \frac{1}{(k_B T)^2} \int_{\epsilon_s}^{\infty} \sigma_{j \to j'}(\epsilon) e^{-\epsilon/k_B T} \epsilon \, d\epsilon, \quad (7)$$

where $\epsilon = E - E_j$ is precollisional translational energy at temperature T, k_B is Boltzman constant, and ϵ_s is the minimum value of the kinetic energy needed to make E_j levels accessible.

B. $\overline{\rm H} - {\rm H}_2$ interaction potential

In the following section, we will present our results for rotational quantum transitions in collisions between H$_2$ and an antihydrogen atom $\overline{\rm H}$, that is

$${\rm H}_2(j) + \overline{\rm H} \to \overline{\rm H} + {\rm H}_2(j'). \quad (8)$$
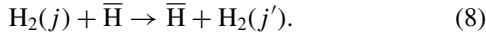
Here H$_2$ is treated as a vibrationally averaged rigid monomer rotor. The bond length was fixed at 1.449 a.u. or 0.7668 Å. The rotation constant of the H$_2$ molecule has been taken as $B_e = 60.8 \, {\rm cm}^{-1}$. The H$_2$ rigid rotor model has been already applied in different publications [31,35–41]. For the considered range of kinetic energies, the model can be quite justified in this special case when only pure rotational quantum transitions at low collisional energies are of interest as in H$_2(j) + \overline{\rm H}$, and when the energy gap between rotational and vibrational energies is much larger than kinetic energy of the collision. In such a model, the quantum mechanical approach is rather simplified.

Next we consider an important physical parameter in atomic and molecular collisions, e.g., the PES between the atoms. There is no global potential energy surface available for the three-atom $\overline{\rm H} - {\rm H}_2$ system. However in Ref. [18], the author calculated the values of interaction energy between H and $\overline{\rm H}$, i.e., the H$-\overline{\rm H}$ energy curve using the Rayleigh-Ritz variational method. Further, the microhartree accuracy of Born-Oppenheimer energies of the system has been achieved in that work.

To construct the H$_2 - \overline{\rm H}$ interaction potential we take the H$-\overline{\rm H}$ energy data from Ref. [18] and make a cubic spline interpolation through all 46 points taken from Table I of that article. These data have been tabulated from $R_{\rm min} = 0.744$ a.u. to $R_{\rm max} = 20.0$ a.u. interatomic distances. Because in the current work, we use the rigid rotor model for H$_2$, we do not need the interaction energy between hydrogen atoms in H$_2$. The three-body interaction potential between a hydrogen molecule and $\overline{\rm H}$ is taken as a sum of two two-body $\overline{\rm H} - {\rm H}$ potential energy curves:

$$V(\vec{r}, \vec{R}) = V(r, R, \Theta) = V_{\rm H - \overline{H}}^{21}(x_{21}) + V_{\rm H - \overline{H}}^{31}(x_{31}), \quad (9)$$

where distances between atoms are written as follow (cf. Fig. 1):

$$x_{21} = \sqrt{r^2/4 + R^2 + rR \cos \Theta}$$

and $$x_{31} = \sqrt{r^2/4 + R^2 + rR \cos(\pi - \Theta)}. \quad (10)$$

TABLE I. Para-H$_2$ rotational spectrum.

Level	Rotational energy (cm^{-1})	Internal quantum momentum in para-H$_2$(j)
1	0.00	0
2	364.80	2
3	1216.00	4
4	2553.60	6
5	4377.60	8
6	6688.00	10
7	9484.80	12
8	12768.00	14
9	16537.60	16
10	20793.60	18
11	25536.00	20
12	30764.80	22
13	36480.00	24
14	42681.60	26
15	49369.60	28
16	56544.00	30
17	64204.80	32
18	72352.00	34
19	80985.60	36
20	90105.60	38
21	99712.00	40
22	109804.80	42
23	120384.00	44
24	131449.60	46
25	143001.60	48
26	155040.00	50
27	167564.80	52
28	180576.00	54
29	194073.60	56

The functions $V_{\overline{\rm H}-{\rm H}}^{k1}(y)$ with $k = 2(3)$ are represented as cubic spline interpolation functions for any value of $y = x_{21}$ or $y = x_{31}$ as follows:

$$V_{\overline{\rm H}-{\rm H}}^{k1}(y) = V_{\overline{\rm H}-{\rm H}}^{k1}(X_i) + B_i(y - X_i)$$
$$+ C_i(y - X_i)^2 + D_i(y - X_i)^3, \quad (11)$$

where $B_i(y - X_i), C_i(y - X_i), D_i(y - X_i)$ perform the spline interpolation and where $X_i \leqslant y \leqslant X_{i+1}$, in each subinterval $[X_i, X_{i+1}]$, $i = 1, 2, 3, \ldots, (n-1)$, $n = 46$. The coordinates X_i and corresponding values of the H$-\overline{\rm H}$ potential energy data have been taken from Table I of Ref. [18]. The calculated potential energy curve is shown in Fig. 2. It is clear that the potential has a singular value when the distance between $\overline{\rm H}$ and H is equal to zero.

The $\overline{\rm H} - {\rm H}_2$ PES which we obtained from Eq. (9) is shown in Fig. 3. Specifically, this potential was used in our calculations of $\overline{\rm H} + {\rm H}_2$ collisions. Again, as seen in Fig. 2 the potential energy curve between $\overline{\rm H} - {\rm H}$ has a Coulomb type singularity at small distances. In our calculations we needed to make additional test runs to achieve convergence in our results. In the next section we will briefly demonstrate the numerical convergence of the results when calculating total elastic-scattering cross sections. These results depend on various numerical and quantum-mechanical scattering parameters.
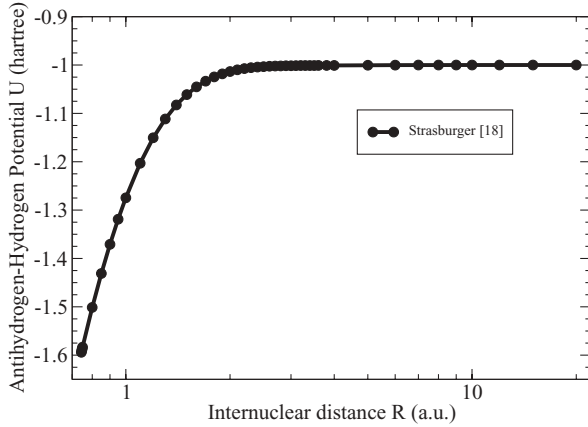
FIG. 2. $\overline{H} - H$ potential energy curve from Ref. [18].

III. RESULT AND DISCUSSION

A. Convergence test

Numerous test calculations have been undertaken to ensure the convergence of the results with respect to all parameters that enter in the propagation of the Schrödinger equation. These include the atomic-molecular distance R, the total angular momentum J, the number of total rotational levels to be included in the close-coupling expansion and others, see Fig. 1. Particular attention has been given to the total number of numerical steps in the propagation over the distance R of the Schrödinger equation (4). Specifically, the parameter R ranges from 0.75 a.u. to 20.0 a.u.. We used up to 50,000 propagation points. We also applied and tested different mathematical propagation schemes included in MOLSCAT.

The rotational energy levels of para-$H_2(j)$ and the corresponding angular momenta j are shown in Table I. The goal of this work is to get new results for $\overline{H}$ + para-H_2 thermal rate coefficients $k_{j \to j'}(T)$ at ultralow temperatures: specifically 0.004 K $< T <$ 4 K. The corresponding cross sections have been calculated for collision energies varying from ~0.0001 cm^{-1} to ~100 cm^{-1}. These energy values are very small. However, despite this fact, to reach convergence of the results we needed to include in expansion (2) a significant number of rotational levels for the H_2 molecule, specifically up to $j_{max} \approx 60$.

In Table II we present results for the total elastic cross sections for two collisional energies: 0.1 cm^{-1} and 0.01 cm^{-1}. The cross sections are shown for a number of different maximum values of the rotational angular momentum $j = j_{max}$ in the H_2 molecule included in expansion (2). This
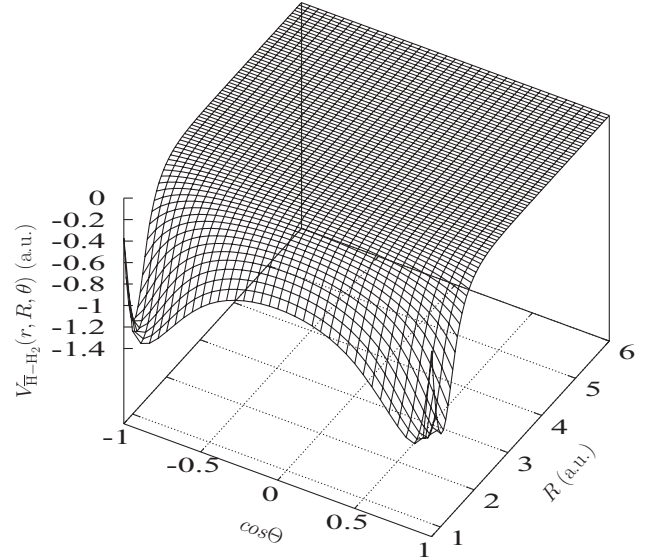
FIG. 3. Interaction potential $V_{\overline{H}-H_2}(r, R, \Theta)$ between $\overline{H}$ and H_2 in a.u. The distance between hydrogen atoms in H_2 is fixed at $r = r(H_2) = 1.449$ a.u.

is the parameter JMAX in MOLSCAT [32]. One can see that JMAX should be at least 56 to achieve convergence. The other scattering parameter in Table II is MXSYM [32]. When we did our test calculations to determine the correct value for the JMAX parameter, the value of the parameter MXSYM was fixed at 24. The parameter MXSYM reflects the number of terms in the potential expansion over angular functions [30,31]. One can see from Table II that in this calculation we need to keep at least 24 terms in the expansion. When we did our test calculations to determine the correct value of the parameter MXSYM the value of JMAX was fixed at 56.

In Table III we present results for total elastic-scattering cross section for a few more selected energies. However, in this table the convergence has been reached by increasing the total angular momentum J. In this table a sufficiently large value of the parameter STEPS (about 10,000) in MOLSCAT was employed so convergence was achieved with respect to the parameter STEPS. As expected, for lower energy collision we needed smaller values for the maximum J. For example, for collision energy $E_{coll} = 0.01$ a.u. it is enough to have $J = 0$; however, $J = 10$ should be taken for $E_{coll} = 100$ a.u.. In Table IV we show the convergence of the elastic-scattering cross section with respect to the number of propagation space steps used in the numerical calculation. One can see from

TABLE II. Total elastic-scattering cross section $\sigma_{el}(10^{-16}$ cm$^2)$ at different collision energies E in (cm^{-1}) in $\overline{H} + H_2 \to H_2 + \overline{H}$ with respect to the maximum value of the rotational angular momentum $j = j_{max}$ in $H_2(j)$ included in the expansion (2) (parameter JMAX in MOLSCAT). Convergence with the number of terms in the potential expansion (parameter MXSYM in MOLSCAT) is also shown. Numbers in parenthesis are powers of 10.

E (cm^{-1})	JMAX					MXSYM			
	30	40	50	56	60	12	20	24	26
0.01	55.4	1.06(3)	6.59(3)	6.56(3)	6.56(3)	1.12(4)	6.75(3)	6.56(3)	6.54(3)
0.1	61.0	5.25(2)	1.59(3)	1.59(3)	1.59(3)	1.97(3)	1.61(3)	1.59(3)	1.59(3)

TABLE III. Total elastic-scattering cross section $\sigma_{el}(10^{-16}$ cm^2) at different collision energies E in (cm^{-1}) in $\overline{H} + H_2 \rightarrow H_2 + \overline{H}$ with respect to the maximum value of the total angular momentum J of the three-atomic system: parameter JTOT in MOLSCAT. Numbers in parenthesis are powers of 10.

E (cm^{-1})	JTOT						
	0	2	4	6	8	10	12
0.01	6.56(3)	6.56(3)					
0.1	1.59(3)	1.59(3)					
1			1.69(2)	1.69(2)			
10			5.85(1)	5.96(1)	5.96(1)		
100					1.65(2)	1.72(2)	1.72(2)

Table IV that we need to include many more propagation points for lower-energy calculations. Specifically, at higher energies we need 500 propagation points, but for lower energies more than 10,000 points are needed to achieve comparable precision. This can be associated with the fact that there is a pronounced resonance in the $\overline{H} + para - H_2$ elastic-scattering cross section at collision energies $\epsilon \sim 3.5 \times 10^{-5}$ Hartree; see Fig. 4. For this reason, in our calculations we need a substantial number of propagation points at lower energies to construct the very large cross sections numerically near the ultralow energy resonance. All the test calculations in Tables III and IV have been done with the appropriate values of the following parameters to achieve convergence: JMAX $= 56$ and MXSYM $= 24$. These appropriate values of parameters have been used in our subsequent calculations for the total elastic $\sigma_{el}(E)$ and rotational quantum state transfer $\sigma_{j \rightarrow j'}(E)$ cross sections and corresponding thermal rate coefficients $k_{j \rightarrow j'}(T)$.

B. $\overline{H}+$ para-H$_2$ results

Now we present computational results for process (8), namely for elastic scattering ($j = 0 \rightarrow j' = 0$) and for low quantum number rotational transitions between levels with $j = 0, 2$ and 4: $2 \rightarrow 0$, $0 \rightarrow 2$, $4 \rightarrow 0$, and $4 \rightarrow 2$. From the results of Table III we see that to reach numerical convergence, for the elastic scattering cross section, we need to include a large number of H$_2$ rotational levels, specifically up to 60.

The results for the elastic-scattering cross sections $\sigma_{el}(\epsilon)$ for $\overline{H} + H_2 \rightarrow H_2 + \overline{H}$ are shown in Fig. 4 together with the corresponding results of variational calculations of Gregory

and Armour [16]. It can be seen, that basically the two sets of cross sections are close to each other, although in our calculations we use a larger number of collision energy points, specifically up to 200. In our calculations a shape resonance is found at energy $\epsilon \sim 3.5 \times 10^{-5}$ hartree. As in Ref. [16] our $\sigma_{el}(\epsilon)$ tends to reach a constant value at lower energies with $\sigma_{el}(\epsilon \lesssim 10^{-8}$ a.u.$) = 9.47 \times 10^3 a_0^2$. This result allows us to calculate the $\overline{H} + H_2$ scattering length, which is

$$a = \sqrt{\sigma_{el}/(4\pi)} = 27.5 a_0. \quad (12)$$

The Gregory-Armour scattering length [16] obtained with a variational method is $\tilde{a} = 19.5 a_0$. The two results are in reasonable agreement with each other. It is pertinent to note here, that such a large elastic-scattering cross section at low energies and a large scattering length is the consequence of the strong Coulomb attraction between hydrogen and antihydrogen atoms at small distances leading to a pronounced ultralow energy resonance.

In Figs. 5(a) and 5(b) we show the total state-resolved cross sections $\sigma_{j=2 \rightarrow j'=0}(v)$ vs. relative velocity v and the corresponding thermal rate coefficients $k_{2 \rightarrow 0}(T)$ vs. temperature T for the hydrogen molecule rotational relaxation process. It is seen, that when the collision energy increases the deexcitation cross section decreases. It can be explained in the following way: at low relative velocities (kinetic energies) between H$_2(j = 2)$ and $\overline{H}$, the rotationally excited H$_2$ molecule has more time for interaction and, consequently, it has higher quantum-mechanical probability to release its internal rotational energy to $\overline{H}$. The resulting corresponding

TABLE IV. Total elastic-scattering cross section $\sigma_{el}(10^{-16}$ cm^2) at different collision energies E in (cm^{-1}) in $\overline{H} + H_2 \rightarrow H_2 + \overline{H}$ with respect to the number of numerical space steps in propagation over distance R of the Schrödinger equation (parameter STEPS in MOLSCAT). Numbers in parentheses are powers of 10.

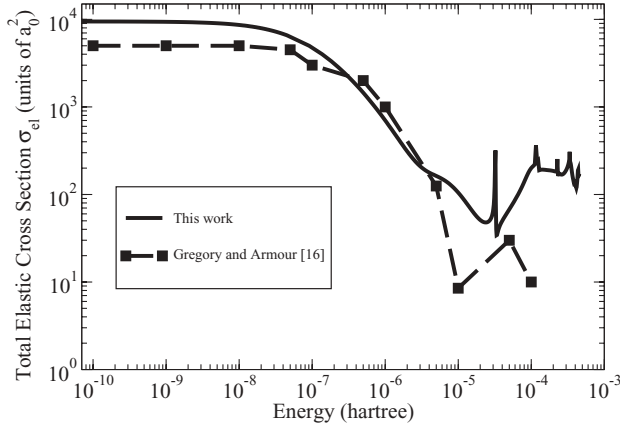| E (cm^{-1})	STEPS						
	500	750	1000	5000	7000	10,000	50,000
0.01	3.62(2)		1.75($-$1)			6.53(3)	6.54(3)
0.1	3.64(2)		2.67			1.60(3)	1.59(3)
1	1.77(2)		1.70(2)	1.70(2)	1.70(2)		
10	6.23(1)		6.00(1)	5.96(1)	5.96(1)		
100	1.72(2)	1.72(2)					

FIG. 4. Total elastic-scattering cross section for $\overline{H} + H_2$ at different energies: results from Gregory and Armour [16] and this work.

rate coefficients have been calculated for a temperature range from 0.004 $K < T < 4$ K and are also presented in Fig. 5 below the cross-section results.

Next, in Figs. 6(a) and 6(b) we present results for the total state-resolved cross sections $\sigma_{j=0 \to j'=2}(v)$ vs. relative velocity v and the corresponding thermal rate coefficients $k_{0 \to 2}(T)$ vs. temperature T for the hydrogen molecule rotational excitation

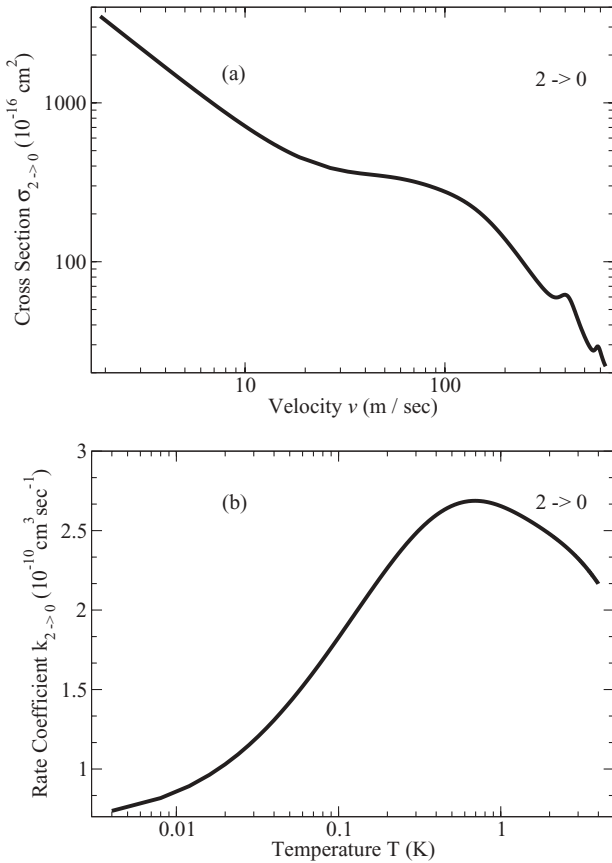FIG. 5. (a) Total state-resolved cross section $\sigma_{2 \to 0}(v)$ vs. relative velocity v. (b) Corresponding thermal rate coefficients $k_{2 \to 0}(T)$ vs. temperature T for the hydrogen molecule rotational relaxation process $H_2(j = 2 \to j = 0)$ in $\overline{H} - H_2$ collision.
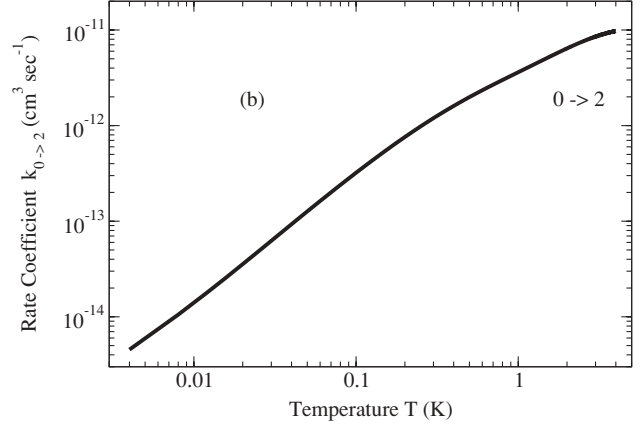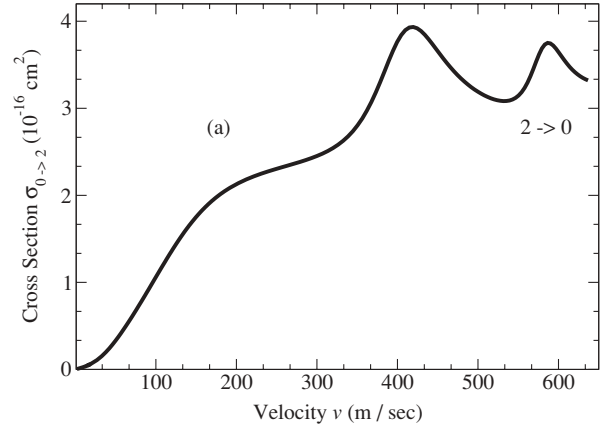

FIG. 6. (a) Total state-resolved cross section $\sigma_{0 \to 2}(v)$ vs. relative velocity v. (b) Corresponding thermal rate coefficients $k_{0 \to 2}(T)$ vs. temperature T for the hydrogen molecule rotational excitation process $H_2(j = 0 \to j = 2)$ in $\overline{H} - H_2$ collision.

process. It is quite understandable, as we find from Fig. 6(a), that when the collision energy (relative velocity v) increases the quantum-mechanical probability and corresponding cross section of the rotational excitation of $H_2(j)$ also increases. Figure 6(b) depicts the corresponding results for the thermal rate coefficient.

In Figs. 7(a) and 7(b) we present results for cross sections and rates for the rotational relaxation process, as in Figs. 5(a) and 5(b), but now connecting the states $j = 4$ and $j' = 2$. Finally, in Figs. 8(a) and 8(b) we present results for cross sections and rates for the rotational relaxation process but now connecting the states $j = 4$ and $j' = 0$. An unexpected result has been found in Fig. 7(a) in the rotational transition cross section $\sigma_{4 \to 2}(v)$, i.e., when the H_2 quantum angular momentum has been changed from $j = 4$ to $j' = 2$. One can see that the values of these cross sections at very low collision energies are almost from 5 to 10 times larger then other cross sections considered in this work as compared with the results from Figs. 5, 6, and 8. Further investigation is needed to understand this phenomenon.

IV. SUMMARY

A quantum-mechanical study of the state-resolved rotational relaxation and excitation cross sections and thermal rate coefficients in ultracold collisions between hydrogen
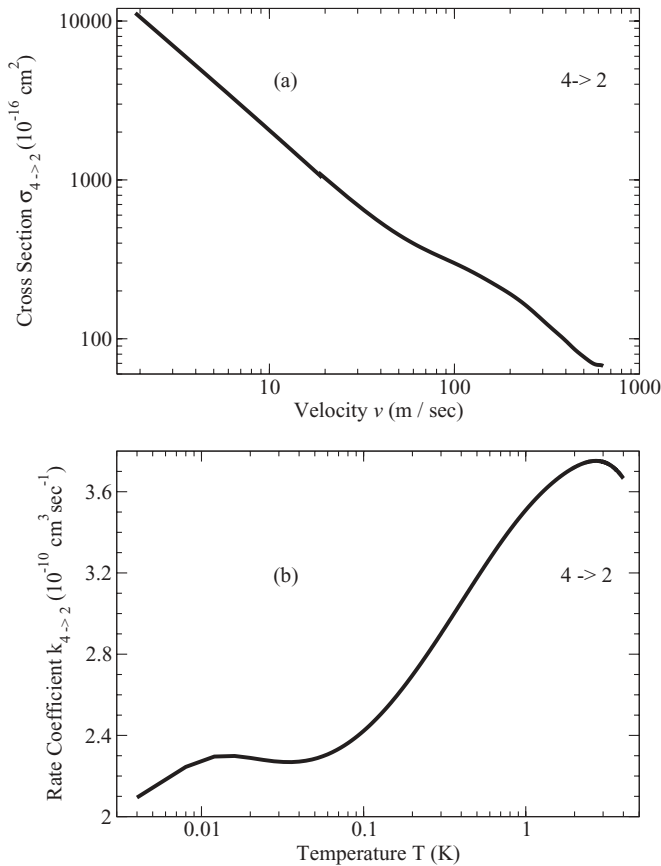
FIG. 7. (a) Total state-resolved cross section $\sigma_{4\to2}(v)$ vs. relative velocity v. (b) Corresponding thermal rate coefficients $k_{4\to2}(T)$ vs. temperature T for the hydrogen molecule rotational relaxation process H$_2(j=4 \to j=2)$ in $\overline{\mathrm{H}} - \mathrm{H}_2$ collision.
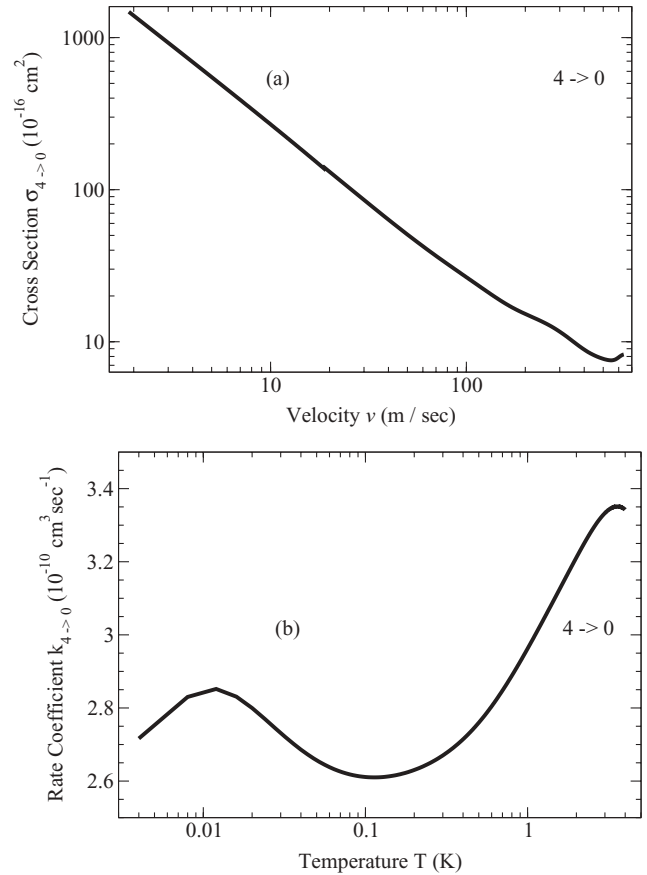

FIG. 8. (a) Total state-resolved cross section $\sigma_{4\to0}(v)$ vs. relative velocity v. (b) Corresponding thermal rate coefficients $k_{4\to0}(T)$ vs. temperature T for the hydrogen molecule rotational relaxation process H$_2(j=4 \to j=0)$ in $\overline{\mathrm{H}} - \mathrm{H}_2$ collision.

molecules H$_2$ and antihydrogen atoms $\overline{\mathrm{H}}$ has been the subject of this work. A model three-body PES for H$_2 - \overline{\mathrm{H}}$ has been constructed as a sum of two two-body H$ - \overline{\mathrm{H}}$ interaction potentials for two different hydrogen atoms. The H$ - \overline{\mathrm{H}}$ results are taken from Ref. [18]. This H$ - \overline{\mathrm{H}}$ interaction potential is shown in Fig. 2. The H$_2 - \overline{\mathrm{H}}$ PES is presented in Fig. 3. Calculation for total elastic-scattering cross section and for low quantum rotational transition states have been performed. We considered only the following quantum transitions: $j = 2 \to j = 0$, $j = 0 \to j = 2$, $j = 4 \to j = 2$, and $j = 4 \to j = 0$.

A test of the numerical convergence was undertaken. These results are presented in Tables II, III and IV. The calculation was performed using the MOLSCAT program [32]. Different propagation schemes included in the MOLSCAT program have been used and tested. Our results for the H$_2(j) + \overline{\mathrm{H}}$ total elastic-scattering cross section are in reasonable agreement with the corresponding results from Gregory and Armour [16]. The authors of this paper used a different PES, which is still unpublished, and applied a quantum-mechanical variational approach. Unfortunately, the rotational transitions in the H$_2(j) + \overline{\mathrm{H}}$ collisions have not been calculated in that work [16].

It is appropriate to compare the H$ + H_2$ system with the $\overline{\mathrm{H}} + \mathrm{H}_2$ system. The strong Coulomb attraction between H

and $\overline{\mathrm{H}}$ in the latter system leads to a low-energy resonance (see, Fig. 4), absent in the former system, which is responsible for the large cross sections at low energies in the present calculation. Also, there will be a large H$ - \overline{\mathrm{H}}$ annihilation cross section in $\overline{\mathrm{H}} + \mathrm{H}_2$, not considered in the present investigation and absent in H$ + H_2$. One of the interesting results of the present work is that the cross section of the rotational transition H$_2(j = 4 \to j = 2)$ at ultralow energies are approximately 5–10 times larger than other transition state cross sections. Further investigation will reveal if this fact is related to some property of the specific PES used in our work.

To the best of our knowledge we do not know of any other calculation of the rotational transitions in the H$_2(j) + \overline{\mathrm{H}}$ collision. These results can help to model energy transfer processes in the hydrogen-antihydrogen plasma and perhaps to design new experiments in the field of the antihydrogen physics. Finally, we believe that in future work it would be useful to include vibrational degrees of freedom of the H$_2$ molecules, i.e., to carry out quantum-mechanical calculations for different rotational-vibrational relaxation processes: H$_2(v, j) + \overline{\mathrm{H}} \to \overline{\mathrm{H}} + \mathrm{H}_2(v', j')$, where v and v' are the vibrational quantum numbers of H$_2$ before and after the collision, respectively. Such new calculations could, perhaps, reveal certain tunneling effects on the interplay between rotational

and vibrational degrees of freedom in the H_2 molecule. Last but not least, a precise full dimensional three-body PES between antihydrogen atom and hydrogen molecule is urgently needed.

[1] R. Landua, Phys. Rep. **403-404**, 323 (2004).

[2] M. H. Holzscheiter, M. Charlton, and M. M. Nieto, Phys. Rep. **402**, 1 (2004).

[3] A. Y. Voronin, P. Froelich, and B. Zygelman, Phys. Rev. A **72**, 062903 (2005).

[4] A. Yu. Voronin and P. Froelich, J. Phys. B **38**, L301 (2005).

[5] G. P. Collins, Sci. Am. **292**, 78 (2005).

[6] M. Amoretti *et al.*, Nature (London) **419**, 456 (2002).

[7] T. W. Hijmans, Nature (London) **419**, 439 (2002).

[8] G. Gabrielse, Adv. At. Mol. Opt. Phys. **50**, 155 (2005).

[9] G. Gabrielse *et al.*, Phys. Rev. Lett. **89**, 213401 (2002); **89**, 233401 (2002); C. H. Storry *et al.*, *ibid.* **93**, 263401 (2004); M. Amoretti *et al.*, *ibid.* **97**, 213401 (2006).

[10] M. M. Nieto, M. H. Holzscheiter, and S. G. Turyshev, e-print arXiv:astro-ph/0410511v1, 21 Oct 2004.

[11] M. H. Holzscheiter and M. Charlton, Rep. Prog. Phys. **62**, 1 (1999).

[12] K. Strasburger and H. Chojnacki, Phys. Rev. Lett. **88**, 163201 (2002).

[13] E. A. G. Armour, M. R. Gregory, and Y. Liu, Nucl. Instrum. Methods Phys. Res. B **247**, 123 (2006); P. K. Sinha and A. S. Ghosh, *ibid.* **266**, 379 (2008); P. Froelich, S. Jonsell, A. Saenz, B. Zygelman, and A. Dalgarno, Phys. Rev. Lett. **84**, 4577 (2000).

[14] J. S. Cohen, J. Phys. B **39**, 3561 (2006).

[15] S. Giorgini *et al.*, Rev. Mod. Phys. **80**, 1215 (2008).

[16] M. R. Gregory and E. A. G. Armour, Nucl. Instrum. Methods Phys. Res. B **266**, 374 (2008).

[17] P. K. Biswas and S. K. Adhikari, Chem. Phys. Lett. **317**, 129 (2000); J. Phys. B **33**, 1575 (2000); **31**, L315 (1998); S. K. Adhikari and P. K. Biswas, Phys. Rev. A **59**, 2058 (1999); S. K. Adhikari, P. K. Biswas, and R. A. Sultanov, *ibid.* **59**, 4829 (1999).

[18] K. Strasburger, J. Phys. B **35**, L435 (2002).

[19] K. Strasburger, J. Phys. B **37**, 4483 (2004).

[20] K. Strasburger, J. Phys. B **38**, 3197 (2005).

[21] E. A. G. Armour and V. Zeman, Int. J. Quantum Chem. **74**, 645 (1999).

[22] P. K. Sinha and A. S. Ghosh, Europhys. Lett. **49**, 558 (2000).

[23] V. Zeman, E. A. G. Armour, and R. T. Pack, Phys. Rev. A **61**, 052713 (2000).

[24] S. Jonsell, A. Saenz, P. Froelich, B. Zygelman, and A. Dalgarno, Phys. Rev. A **64**, 052712 (2001).

[25] E. A. G. Armour and C. W. Chamberlain, J. Phys. B **35**, L489 (2002).

[26] P. K. Sinha, P. Chaudhuri, and A. S. Ghosh, Phys. Rev. A **67**, 052509 (2003).

[27] M. M. Nieto, M. H. Holzscheiter, and T. J. Phillips, J. Optics B **5**, S547 (2003).

[28] L. Labzowsky, D. Solovyev, V. Sharipov, G. Plunien, and G. Soff, J. Phys. B **36**, L227 (2003); C. Y. Hu and D. Caballero, *ibid.* **35**, 3879 (2002); E. Cubero, M. Orozco, P. Hobza, and F. J. Luque, J. Phys. Chem. A **103**, 6394 (1999); P. Hobza, V. Spirko, Z. Havlas, K. Buchhold, B. Reimann, H. D. Barth, and B. Brutschy, Chem. Phys. Lett. **299**, 180 (1999); P. Hobza and Z. Havlas, *ibid.* **303**, 447 (1999).

[29] A. M. Arthurs and A. Dalgarno, Proc. R. Soc. A **256**, 540 (1963).

[30] S. Green, J. Chem. Phys. **70**, 4686 (1979).

[31] S. Green, J. Chem. Phys. **62**, 2271 (1975).

[32] J. M. Hutson and S. Green, *MOLSCAT Computer code, version 14*, (Collaborative Computational Project 6 of the Engineering and Physical Sciences Research Council, Daresbury Laboratory, UK, 1994).

[33] L. D. Landau and L. M. Lifshitz, *Quantum Mechanics: Non-Relativistic Theory*, 3rd ed. (Elsevier, Amsterdam, 1981), Vol. 3.

[34] G. D. Billing and K. V. Mikkelsen, *Molecular Dynamics and Chemical Kinetics* (Wiley Interscience, New York, 1996).

[35] S. Green, J. Chem. Phys. **67**, 715 (1977).

[36] J. Schaefer, Astron. Astrophys. Suppl. Ser. **85**, 1101 (1990).

[37] D. R. Flower, Mon. Not. R. Astron. Soc. **297**, 334 (1998).

[38] E. Roueff and D. R. Flower, Mon. Not. R. Astron. Soc. **305**, 353 (1999).

[39] R. A. Sultanov and D. Guster, Chem. Phys. **326**, 641 (2006). Note that in Eq. (1) of this work the momentum operators should be squared and the equation should look as follows: $(\frac{P_{\vec{R}}^2}{2M_{12}} + \frac{L_{\hat{r}_1}^2}{2\mu_1 r_1^2} + \frac{L_{\hat{r}_2}^2}{2\mu_2 r_2^2} + V(\vec{r}_1, \vec{r}_2, \vec{R}) - E)\Psi(\hat{r}_1, \hat{r}_2, \vec{R}) = 0$, as Eq. (2) in Ref. [41].

[40] R. A. Sultanov and D. Guster, Chem. Phys. Lett. **428**, 227 (2006); **436**, 19 (2007).

[41] R. A. Sultanov, A. V. Khugaev, and D. Guster, Chem. Phys. Lett. **475**, 175 (2009).